ACS APPLIED MATERIALS & INTERFACES

Research Article

www.acsami.org

# Peptide–Graphene Interactions Enhance the Mechanical Properties of Silk Fibroin

Yuan Cheng,[†,∥] Leng-Duei Koh,[‡,§,∥] Dechang Li,[⊥] Baohua Ji,[⊥] Yingyan Zhang,[¶] Jingjie Yeo,[†] Guijian Guan,[†,‡] Ming-Yong Han,[*,‡,§] and Yong-Wei Zhang[*,†]

[†]Institute of High Performance Computing, A*STAR, Singapore 138632, Singapore

[‡]Institute of Materials Research and Engineering, A*STAR, Singapore 117602, Singapore

[§]Department of Biomedical Engineering, National University of Singapore, Singapore 117575, Singapore

[⊥]Biomechanics and Biomaterials Laboratory, Department of Applied Mechanics, Beijing Institute of Technology, Beijing 100081, China

[¶]School of Computing, Engineering, and Mathematics, Western Sydney University, Locked Bag 1797, Penrith NSW 2751, Australia

Supporting Information

**ABSTRACT:** Studies reveal that biomolecules can form intriguing molecular structures with fascinating functionalities upon interaction with graphene. Then, interesting questions arise. How does silk fibroin interact with graphene? Does such interaction lead to an enhancement in its mechanical properties? In this study, using large-scale molecular dynamics simulations, we first examine the interaction of graphene with several typical peptide structures of silk fibroin extracted from different domains of silk fibroin, including pure amorphous (P1), pure crystalline (P2), a segment from N-terminal (P3), and a combined amorphous and crystalline segment (P4), aiming to reveal their structural modifications. Our study shows that graphene can have intriguing influences on the structures formed by the peptides with sequences representing different domains of silk fibroin. In general, for protein domains with stable structure and strong intramolecular interaction (e.g., $\beta$-sheets), graphene tends to compete with the intramolecular interactions and thus weaken the interchain interaction and reduce the contents of $\beta$-sheets. For the silk domains with random or less ordered secondary structures and weak intramolecular interactions, graphene tends to enhance the stability of peptide structures; in particular, it increases the contents of helical structures. Thereafter, tensile simulations were further performed on the representative peptides to investigate how such structure modifications affect their mechanical properties. It was found that the strength and resilience of the peptides are enhanced through their interaction with graphene. The present work reveals interesting insights into the interactions between silk peptides and graphene, and contributes in the efforts to enhance the mechanical properties of silk fibroin.

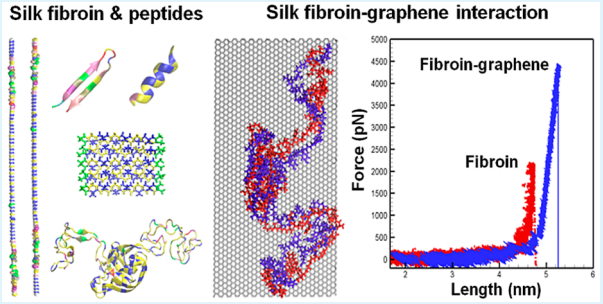


**KEYWORDS:** *silk fibroin, graphene, molecular dynamics, hydrogen bonding, structures, mechanical property*

## 1. INTRODUCTION

Silkworm silk fibroin exhibits a number of superior properties in strength, toughness, biocompatibility, and biodegradability, and its versatile processability further allows its fabrication into various forms such as sponges, hydrogels, films, mats, and particles. These amazing characteristics have enabled a wide range of applications in apparel/medical textiles, surgical sutures, tissue engineering scaffolds, drug/gene carriers, optical components, and sensors.[1−8] As a semicrystalline biopolymer, silk fibroin is composed of nanosized $\beta$-sheet crystallites embedded in an amorphous matrix,[9,10] as shown in Figure 1, panels a and b. The crystalline domains are hydrophobic (i.e., water-hating), while the amorphous domains are hydrophilic (i.e., water loving). It is now known that the mechanical characteristics of silk fibroin are predominantly dictated by the interactions within and between the two types of domains as building blocks and are also influenced by their hydration levels.[11−14] Inspired by the world's strongest and toughest natural silk, that is, the spider dragline silk with a similar hierarchical structure to silkworm silk, a great deal of research effort has been made to enhance the mechanical properties of silkworm silk. So far, various physical, chemical, and biological approaches have been proposed and implemented to enhance the mechanical properties of silkworm silk by manipulating its molecular structures and molecular bonding interactions.[15,16] For example, silk fibroin structures were modulated by controlling the reeling speed for improving their mechanical properties.[17] The coexpression of spider silk proteins via gene transfection also led to the enhancement in mechanical properties via tuning interchain interactions of silk fibroin.[18]

**Received:** June 24, 2015
**Accepted:** September 14, 2015
**Published:** September 14, 2015





DOI: 10.1021/acsami.5b05615
ACS Appl. Mater. Interfaces 2015, 7, 21787−21796

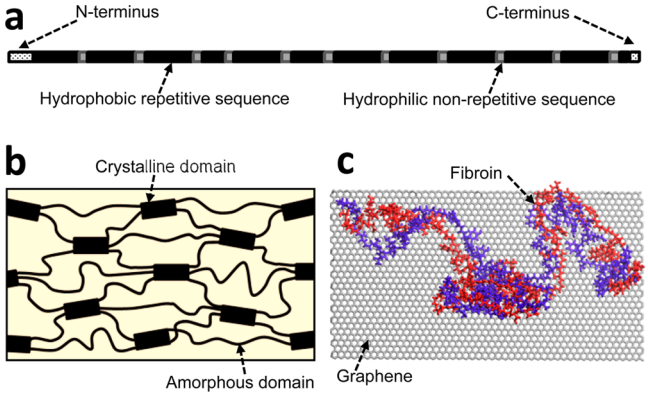


**Figure 1.** Schematics of (a) a full-length silk protein covering both C and N termini, (b) the silk fibroin structure, and (c) the silk–graphene interaction.

Graphene and its derivatives have been widely used as fillers to reinforce polymer composites due to their outstanding mechanical properties, large surface area, high flexibility, and remarkable processability.[19−25] Studies have further revealed that graphene and its derivatives can form various noncovalent bindings to biomolecules,[26−29] and such interactions can lead to the secondary structure changes of biomolecules. Silk fibroin is a multiblock copolymer with backbones comprising alternating hydrophilic and hydrophobic domains at nanoscale, facilitating various hydrogen bond, polar–polar, and hydrophobic–hydrophobic interactions. Then, several questions arise naturally. How does graphene interact with silk fibroin? What changes occur in the structure and conformation of silk fibroin upon the interactions? In what way do the interactions change the mechanical properties? It is clear that insightful answers to the questions provide not only significant scientific value to understand the fundamental interactions between biomolecules and graphene, but also great engineering impact to modulate the mechanical properties of silk fibroin.

Molecular simulations and theoretical analyses have been widely utilized to investigate the interactions of various types of nanoscale materials with proteins or peptides[30−35] such as the adhesion of low dimensional carbon nanomaterials to F-actin networks.[36] In this research, we investigate the interaction of graphene with silk fibroin using molecular dynamics (MD) simulations. We first choose representative sequences of peptides from the crystalline domain, amorphous domain and N-terminal of silk fibroin, and one segment of silk fibroin combining both amorphous and crystalline domains, as illustrated in Figure 1, panel c, to study their interactions with graphene and examine the effects on the structural changes of silk fibroin. Our simulation results show that graphene exerts remarkable effects on the molecular conformation of these representative sequences of silk fibroin. Subsequently, tensile tests are performed to examine the mechanical properties of the selected sequences in terms of strength and resilience of these typical silk fibroin segments with and without interaction with graphene. Our research not only provides in-depth understandings in their interacting mechanisms, but also offers a possible route for engineering the molecular structure of silk fibroin to greatly enhance its mechanical properties.

## 2. MODELS AND METHODS

**2.1. Peptides from the Different Domains of Silk Fibroin.** Silkworm silk fibroin heavy chain protein includes 5000+ residues of amino acids,[37] and thus it is not computationally feasible to obtain the native structure of the whole molecule and investigate the protein–graphene interaction via MD simulations. Hence, we select four representative peptide sequences of silk fibroin to study the interaction between silk fibroin and graphene substrate. In the following, we describe the molecular sequences of the four peptides labeled as P1, P2, P3, and P4, the first three of which are from the crystalline domain, amorphous domain, and N-terminal of silk fibroin, respectively, while P4 is a combination of the amorphous and crystalline domains.

As shown in Figure 2, panel a, P1 consists of four identical sequences of GAGAGAGAGAGTGS, which is a common component

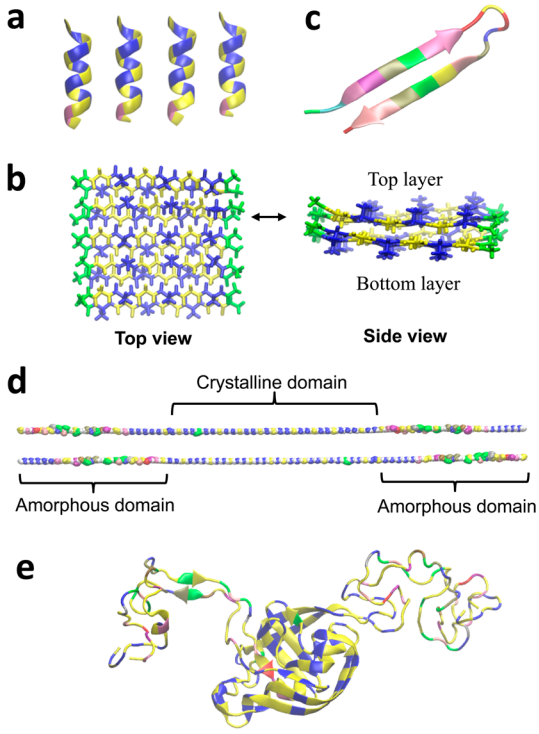


**Figure 2.** Initial peptide structures: (a) P1, (b) P2, (c) P3, and (d) P4. These initial structures of peptides are adopted for our simulations with and without graphene substrate in a water environment. (e) Pre-equilibrated structure of P4 adopted for simulating its interaction with graphene substrate in explicit water solvent.

in a helical or coil form in the amorphous domain of silk fibroin.[37] Here, we adopt the helical form as the initial structure, which is constructed using Software package SYBYL 8.0 (Tripos Associates, Inc.).

As shown in Figure 2, panel b, P2 is a two-layer $\beta$-sheet crystallite, which is extracted from the structure of Protein Data Bank entry: 2SLK.[38] In each layer, there are five peptide chains, with each having the same sequence of GAGAGA.

As shown in Figure 2, panel c, P3 is extracted from the N-terminal of silk fibroin, which is known to play an important role in the structural assembly as well as the mechanical properties of silk fibroin.[8,39] The molecular structure is available in Protein Data Bank with the entry: 3UA0.[39] The initial configuration of P3 includes both $\beta$-sheet and random coil configurations. The residue numbers are 81–101 with the sequence of IKTFVITTDSDGNESIVEDV.

As shown in Figure 2, panel e, P4 is a multidomain silk peptide consisting of two amorphous domains and one crystalline domain, and its complete sequence is provided in the Supporting Information. The crystalline domain includes repeating units of poly(GA) and GAGAS, while there are two amorphous domains (also known as linkers) on each side of the crystalline domain. These three different parts were named as linker 5, domain 6.5, and linker 6 in the literature.[37] It should be noted that the equilibrium molecular structure of P4 is not


DOI: 10.1021/acsami.5b05615
ACS Appl. Mater. Interfaces 2015, 7, 21787−21796

available in Protein Data Bank. Therefore, the initial structure is built based on an extended initial structure, which contains two antiparallel fully extended chains with an initial distance of 5 Å between them, as shown in Figure 2, panel d. To obtain the initial structure, we first carry out stochastic dynamics simulation for 50 ns within an implicit water solvent environment. Subsequently, the pre-equilibrated configuration is solvated in a water box, and equilibrated MD simulation is carried out for another 20 ns to obtain the initial structure, as shown in Figure 2, panel e.

**2.2. Simulation Methods for Peptide–Graphene Interactions.** The AMBER99 force field[40] is adopted to parametrize the peptides and the nonbonded interactions between the peptides and graphene. The interaction between the carbon atoms in graphene is described by a Morse potential, a harmonic cosine of the bending angle, a two-fold torsion potential, and a van der Waals (VDW) interaction with an equilibrium distance of $\sigma_{cc}$ = 3.40 Å and potential well depth of $\varepsilon_{cc}$ = 0.086 kcal mol$^{-1}$, corresponding to sp$^2$ carbons in the AMBER99 force field. VDW parameters between different types of atoms are calculated from the parameters of the pure atoms using combination rules.[41] The potential functions and parameters adopted here are well-accepted and have been validated by many studies, including those on carbon nanotubes in water,[42,43] and on interactions between carbon nanotube/graphene and biomolecules.[31,44] Similar parameters and simulation approaches have also been utilized to investigate the mechanical properties of silk crystalline in earlier studies.[12−14,45]

All simulations are carried out using the package Gromacs 4.5.4.[46] Periodic boundary conditions and a time step of 0.001 ps are adopted. MD simulations are performed using the NPT ensemble at temperature of $T$ = 300 K and pressure of $P$ = 1 bar. The particle mesh Ewald (PME) method is used to calculate the long-range electrostatic interactions.[47] The figures for peptides and graphene structures are generated using the visual molecular dynamics (VMD) code.[48] To analyze the simulation results, protein secondary structures are calculated using the STRIDE algorithm,[49] which is a built-in module in the VMD Molecular Graphics Viewer.

To study the interactions of the peptide–graphene complex, for each case in a water environment, MD simulations are performed on the peptide–graphene complex in a water box. In all the simulations, the TIP3P water box is adopted.[50] Initially, the peptides are placed very close to graphene with a distance of around 5 Å, thus to allow spontaneous adsorption of the peptides onto the surface of graphene. To study the interactions of peptide–graphene complex for each case, energy minimization is carried out first on the whole system, then the backbone of the peptide is restrained and MD simulations were carried out for 1 ns, and water molecules are equilibrated simultaneously. Subsequently, MD simulations are performed with no restrain applied on the peptides. The graphene substrate is fixed throughout the simulations.

The graphene substrate with the dimensions of 8.2 × 4.0 nm$^2$ is used for P1, P2, and P3. For P4, a larger graphene substrate with dimensions of 11.31 × 6.00 nm$^2$ is used. When solvated in water boxes with graphene, the systems of P1, P2, P3, and P4 consist of 23 665, 21 782, 30 783, and 53 309 atoms, respectively.

**2.3. Simulation Method for Mechanical Testing.** Since the interaction between silk fibroin and graphene may lead to changes in silk fibroin molecular structures, we would like to examine this effect on the mechanical behavior of silk peptide structures. Because of the large size of P4, it is not feasible to perform mechanical testing simulation on this system. Instead, tensile tests are carried out for P1 and P3, and pull-out tests for P2 using steered molecular dynamics (SMD) simulations.[51] For pull-out tests on P2, to pull the targeted chain away, the terminal residues are subjected to a force along the chain direction by pulling a spring with a constant velocity. A counter force is applied to the rest of the chains. A pulling rate of 0.2 nm/ns with a spring constant of 830 pN/nm is used for all the SMD simulations.

## 3. RESULTS AND DISCUSSION

**3.1. Influence of Graphene Substrate on Peptide Structures.** *3.1.1. Representative Peptide-P1.* MD simulations are performed to examine the molecular structural change of P1 in the absence or presence of graphene substrate in the explicit water box. The respective configurations of P1 after 50 ns of equilibration are shown in Figure 3, panels a and b,

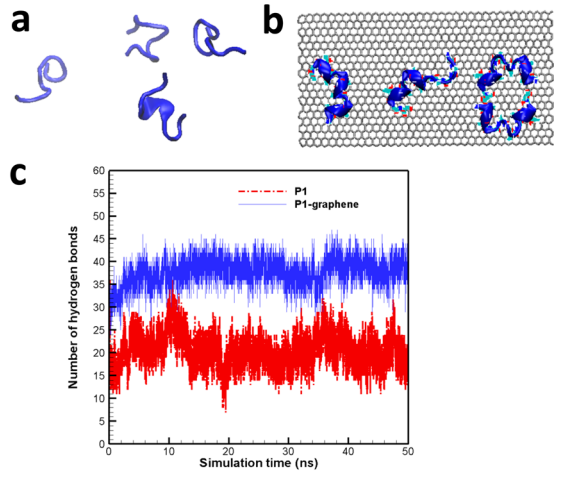


d

| | P1 | P1-graphene |
|---|---|---|
| Contents of Helix Structure (including α-helix & 3-10 helix) (%) | 1.79±0.38 | 48.21±2.79 |

**Figure 3.** Snapshots of P1 peptide structure after 50 ns of equilibration (a) in water and (b) on graphene in water. (c) Hydrogen-bond number as a function of simulation time. (d) Helical structure content without and with the presence of graphene substrate. The rest of the components are mainly random coil structures.

respectively. A quantitative examination of the number of hydrogen bonds shows that the mean number of hydrogen bonds in P1 with graphene is higher than that without graphene, as shown in Figure 3, panel c. Also, as shown in the table in Figure 3, panel d, the percentage of helical structure without graphene is only 1.79%; however, the value increases to 48.21% with graphene. Hence, the presence of graphene promotes the formation of helical structures. Here, it should be noted that the helical structures includes both $\alpha$-helix (i.e., 4 residues per helical turn) and the $3_{10}$-helix (i.e., 3 residues per helical turn). This observation is consistent with a previous study,[26] in which a dodecamer peptide was found to predominantly adopt $3_{10}$-helical conformation upon adsorption to graphene surface.

To further understand the structure changes in P1 upon interaction with graphene, we examine the time-evolution of structure components without and with the presence of the graphene substrate, and the results are depicted in Figure 4, panels a and b, respectively. It can be seen that the graphene substrate plays the role of promoting the formation of $3_{10}$ -helices. For each peptide sequence, approximately three $3_{10}$-helical turns per peptide sequence were formed. Compared to the system without graphene where P1 mainly adopted the turns and coils structure with occasional transient formation of helices (i.e., both $\alpha$- and $3_{10}$-helices), in the presence of graphene substrate, P1 mainly adopted the conformation of $3_{10}$-helices throughout the 50 ns of equilibrium simulation. Note


DOI: 10.1021/acsami.5b05615
ACS Appl. Mater. Interfaces 2015, 7, 21787−21796

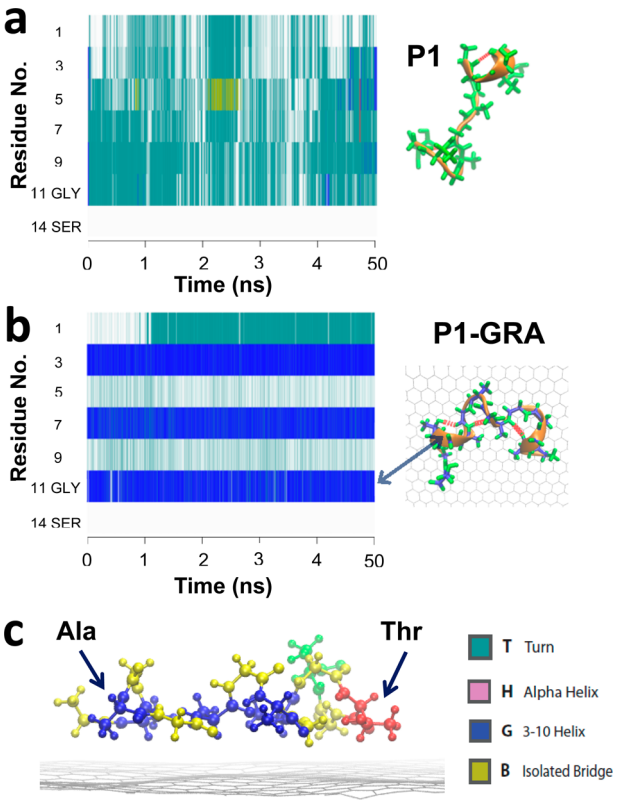


**Figure 4.** Time-evolution of the P1 secondary structures (a) without graphene and (b) with graphene. Different colors in the time-evolution graphics represent different types of secondary structures. In particular, the continuous blue color bars in panel b demonstrate the stable helical structure in P1 throughout the equilibrium simulation. (c) Side view of the interaction between P1 and graphene, where Ala residues are displayed in blue, Gly in yellow, Thr in red, and Ser in green.

that the $3_{10}$-helix is defined by $i + 3 \rightarrow i$ hydrogen bonding (i.e., the N−H group of the amino acid residue forms a hydrogen bond with the C=O group of the amino acid three residues earlier), as compared to $i + 4 \rightarrow i$ hydrogen bonding in an $\alpha$-helix. Hence, the structural changes from coils and transient helices to stable $3_{10}$-helices account for the increase in the number of hydrogen bond in P1 upon the adsorption onto graphene.

At equilibrium, the average VDW interaction energy between P1 and graphene substrate is about −1250 kJ/mol, as shown in Figure 5, with P1 binding to graphene mainly via the hydrophobic side chains on Ala or Thr residue. As shown in the structure time-evolution (Figure 4b), the $3_{10}$-helices are consistently formed from the sequences Ala-Gly-Ala (i.e., residue no. 2−4, 6−8) or Ala-Gly-Thr (i.e., residue no. 10−12). Necessarily, the binding of both methyl groups (i.e., Ala side chains) in the sequence (e.g., Ala-Gly-Ala) to graphene (while the methyl-deficient Gly is left unbound) gives rise to a helical turn (in this case, a $3_{10}$-helical turn). It was observed that a sequence having a methyl-deficient amino acid (e.g., Ser) in place of one of the methyl-containing Ala/Thr does not form any helical structure, that is, the last three residues in the P1 sequence (i.e., Thr-Gly-Ser) have not formed helical structure at all time during its interaction with the graphene substrate (Figure 4c). The hydrophobic methyl ($-CH_3$) group in the side chains of these amino acid residues appears to be the main factor that drives the formation of the $3_{10}$-helices via its hydrophobic interaction with graphene substrate, which is also hydrophobic in nature. Such hydrophobic interactions could be critical to the formation of the helices on graphene substrate.

Because of the higher number of hydrogen bonds, the higher percentage, and also the more stable helical structures arising from the VDW interaction between P1 and graphene, it is expected that the modified molecular structure of the fibroin peptide be more stable and thus exhibit enhanced mechanical properties.

*3.1.2. Representative Peptide-P2.* It is known that the crystalline domain of silk fibroin, which mainly consists of $\beta$-sheets crystallite structure, dictates the strength of the silk fibroin.[13] Representative snapshots of P2 adsorbed onto graphene substrate at equilibrium are shown in Figure 6, panels a and b. It can be seen that overall the $\beta$-sheet configuration is well maintained. A previous study[13] showed that the interchain interaction between $\beta$-chains in the crystallite is strong. Upon the adsorption of P2 on graphene substrate, the VDW interactions between P2 and graphene compete with the interactions between peptide chains. As

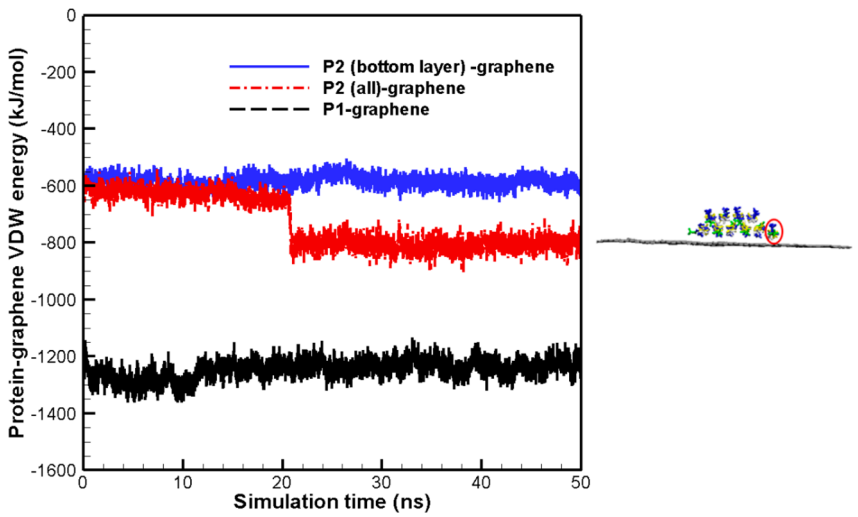


**Figure 5.** VDW interaction energies between P1 and graphene (black curve), between both layers of P2 and graphene (red curve), and between the bottom layer of P2 and graphene (blue curve) as a function of simulation time.


DOI: 10.1021/acsami.5b05615
ACS Appl. Mater. Interfaces 2015, 7, 21787−21796

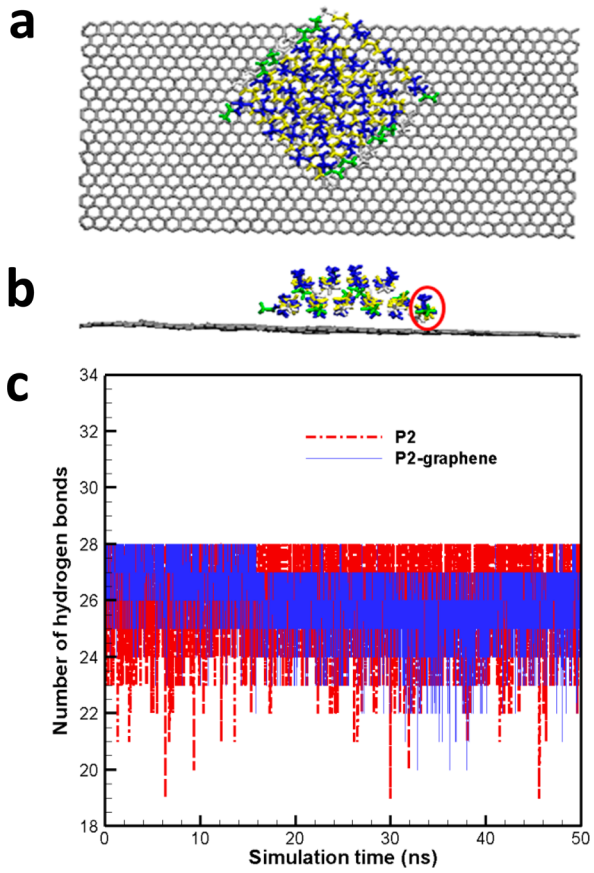


**Figure 6.** Snapshots of P2 on graphene after 50 ns of equilibration. (a) Top view and (b) side view. Attracted on the graphene substrate, one of the $\beta$-chains on the top layer moves down to the bottom layer (highlighted in red circle). (c) Number of hydrogen bonds in the bottom layer with (blue curve) and without (red curve) graphene as a function of simulation time.

shown in Figure 6, panel b, attracted by the graphene substrate, one of the $\beta$-chains (highlighted by red circle) on the top layer moves down to the bottom layer during equilibrium. Corresponding to the change in the $\beta$-chain position, the total VDW energy between the peptide structure and graphene is reduced, indicating a stronger binding affinity between them, as shown in red curve in Figure 5.

To further understand their interactions, we mainly focus on the behaviors of the bottom layer of P2 adsorbed directly to the graphene surface, excluding the shifted peptide chain from the top layer. On the basis of the data shown in Figure 6, panel c, the mean number of hydrogen bonds without graphene substrate is 25.99 ± 1.36, while that with graphene is 25.60 ± 1.23 (both are averaged over the last 10 ns of simulation time). At the initial stage of the interaction, the hydrogen-bond number in the bottom layer dropped slightly and then maintained at a lower value with small fluctuation. The standard deviation of the hydrogen bond number with graphene is smaller than that without graphene. Thus, the mean number of the hydrogen bonds in the bottom layer is relatively insensitive to the presence of graphene, albeit with smaller fluctuations in the number of hydrogen bonds with graphene. Hence, these results clearly show that the $\beta$-sheets crystallite is a very stable configuration, and the influence of graphene substrate on its molecular structure is insignificant.

*3.1.3. Representative Peptide-P3.* The initial structure of P3 in this case includes both $\beta$-sheet and random coil configurations, and the representative snapshots of the equilibrium structure of P3 without and with the presence of graphene substrate are shown in Figure 7, panels a and b. It can

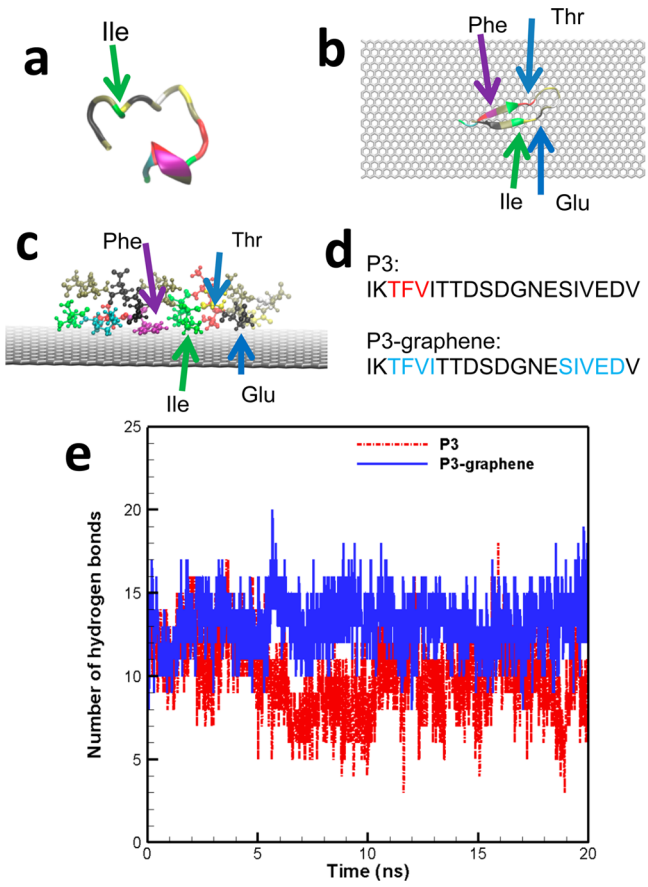


**Figure 7.** Representative snapshots of P3 at equilibrium (a) in water only and (b) on graphene in water. The green arrows highlight the domains dominated by random coil structures in water, while on graphene substrate, the $\beta$-sheet domain is still maintained. Residues Thr, Glu, and Phe are highlighted. (c) Side view of P3 adsorbed to the graphene. (d) Illustration of the sequence of P3 representative structures, where residues in blue denote those in $\beta$-sheet configuration, those in red represent helical structure, while those in black are in other types of secondary configuration. (e) Hydrogen-bond numbers with and without graphene as a function of the simulation time.

be seen from Figure 7, panel a that P3 predominantly forms random coils in water despite containing $\beta$-sheet forming sequences. However, the graphene substrate helps in retaining some fraction of $\beta$-sheet configuration in water, as shown in Figure 7, panels b–d. As an example, the locations of the same residue (ILE16) are highlighted with green arrows in Figure 7, panels a and b, where a random coil structure is adopted without the graphene substrate (Figure 7a), while the same residue remains in $\beta$-sheet configuration with the graphene substrate (Figure 7b,c). The secondary structures of the residues in each case are represented by different colors, as shown in Figure 7, panel d. The residues in red represent the helical domain of P3 in water without the presence of graphene substrate, while those in blue represent the residues in $\beta$-sheet structures in the presence of graphene substrate. Residues in


DOI: 10.1021/acsami.5b05615
ACS Appl. Mater. Interfaces 2015, 7, 21787–21796

other types of secondary structures are displayed in black. The residues that may have strong binding affinities to the graphene substrate are also illustrated in Figure 7, panels b and c (e.g., methyl-containing side chain of Thr, the $-CH_2CH_2-$ group of Glu, and the aromatic ring on Phe), and all bind strongly to the graphene (Figure 7c).

The hydrogen-bond numbers in P3 for the cases with and without graphene as a function of time are illustrated in Figure 7, panel e. The mean value of hydrogen-bond number calculated during the last 10 ns of simulation increases from 9.97 ± 2.09 (without graphene) to 13.20 ± 1.63 (with graphene). Therefore, the P3-graphene interaction also plays the role of maintaining the hydrogen bonds, thus partially keeping the $\beta$-sheet structure of P3 from being denatured by thermal fluctuations in water solvent. With the enhanced structural stability, P3 is also expected to have stronger mechanical properties upon adsorption onto the graphene substrate.

*3.1.4. Representative Peptide-P4.* For proteins with larger size and involving different types of domains, protein–graphene interactions can be much more complicated. For example, there can be multiple layers of protein adsorbed onto the graphene substrate, and the influence of the substrate on protein subdomains located on different layers of adsorbed protein can also be different. In the present work, the P4 peptide structure, which is extracted from silk fibroin molecule with a much larger size that contains both the crystalline and amorphous domain sequences, is selected to investigate the influence of graphene substrate on the changes of peptide structural contents when adsorbed onto the graphene substrate.

The representative equilibrium configurations of P4 without and with the presence of the graphene substrate are shown in Figure 8, panels a and b, respectively. Compared to P4 without the graphene substrate, more helical structures are observed in the presence of the graphene substrate. Note that helical structures are mainly formed in the amorphous domains located at the two ends of P4 (as shown in the highlighted domains in Figure 8a,b), and the mechanism is similar to that discussed in the P1-graphene interaction. The percentages of different types of structural components are listed in Table 1,

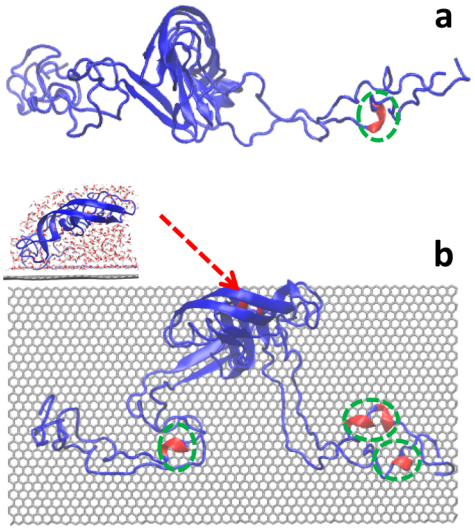


**Figure 8.** Representative snapshots of P4 structure at equilibrium (a) in water only and (b) on graphene in water. The inset shows the side view of water molecules intercalating between P4 and graphene in the domain highlighted with an arrow. Helical secondary structures are highlighted in red and by green circles.

**Table 1. Secondary Structure Contents of P4 without and with the Graphene Substrates**

| | structure types | |
|---|---|---|
| contents of secondary structure (%) | P4 | P4-graphene |
| $\beta$-sheets | 23.78 ± 6.14 | 18.70 ± 1.66 |
| helices | 1.40 ± 0.40 | 4.07 ± 1.10 |
| turns | 36.82 ± 3.33 | 37.09 ± 3.20 |
| random coils | 36.47 ± 6.00 | 36.87 ± 3.33 |

which are obtained based on the configuration data collected during the last 10 ns of simulation time. As shown in Table 1, the percentage of helical structures in the presence of graphene substrate is 4.07%, slightly higher than that without the graphene, which is 1.40%. On the other hand, the content of $\beta$-sheet drops from 23.78% to 18.70% in the presence of graphene substrate. We find that without the presence of graphene substrate, the crystalline domain located in the central part of P4 has a compact and stable configuration. Upon the adsorption to the substrate, the $\beta$-sheet content drops slightly due to the competition between P4-graphene interaction and the inter-$\beta$-chain interaction within P4. These observations are consistent with our findings in the earlier section.

*3.1.5. Discussion.* Our study clearly demonstrates that the influence of the graphene substrate on the adsorbed peptide structures depends on the stability of the peptide structures and the peptide–graphene binding strength as well. For example, both P1 and P3 peptide structures exhibit a random configuration in water solvent, implying that these structures have relatively weak structural stability. For such peptide domain with random structure and weak intramolecular interaction, graphene tends to enhance their stability and increase the number of hydrogen bonds within peptides, that is, both P1 and P3 attain ordered structures when adsorbed onto the substrate, either in helical or $\beta$-sheet configuration, which increases their number of hydrogen bonds. However, crystalline domain of P2 has a very stable structure in water environment, and their stability is only perturbed slightly by the P2–graphene interaction. Correspondingly, there is a slight drop in the number of hydrogen bonds within P2. Considering the interactions between the whole silk fibroin and graphene, graphene has hydrophobic interaction especially with the hydrophobic domains, and the hydrophilic domains of silk fibroin get closer and thus increase the number of hydrogen bonds within protein.[52] Overall, the influence of graphene on peptides extracted from different domains of silk fibroin varies with the sequence, hydrophobicity, and the structure of the peptides. For silk fibroin, the amorphous domain is more sensitive to the influence of the graphene substrate, the crystalline domain was less affected by the substrate, and the N-terminal is in the intermediate.

All simulations are carried out in water environment, equivalent to solution state, to take into account the effect of water since the loading of silk fibroin to graphene is usually performed with a wet process. The water environment does play an important role in promoting the interaction of protein with graphene to form their aggregates, especially between the hydrophobic domains of proteins and graphene.[52]

With the hydrophobic nature of the graphene, the peptides interact with the graphene mainly via the hydrophobic side


DOI: 10.1021/acsami.5b05615
ACS Appl. Mater. Interfaces 2015, 7, 21787–21796

chains of their amino acids. The density of water molecules around the peptide at the interface is much lower than that in bulk water, indicating negligible hydration at the interface. It is possible that water molecules can intercalate at the peptide–graphene interface, at certain regions, especially when the protein has hydrophilic amino acids in the sequence. It is more obvious for a larger sized peptide domain (Figure 8b). For those peptide domains that are not directly adsorbed to graphene surface, the space between graphene and peptide domain indicated by the arrow in the inset of Figure 8, panel b is filled with water molecules. For silk fibroin, hydrating water serves as a plasticizer,[53] which enhances its flexibility and plasticity by promoting chain mobility while reducing its strength by weakening interchain hydrogen bonds.[13] Owing to the peptide–graphene interaction, the weakening effect of hydration on the hydrogen bonds in silk was not observed. Conversely, the silk structures show increased number of hydrogen bonds due to more ordered structures induced by the interaction with graphene.[54]

**3.2. Effects of Graphene Substrate on Mechanical Properties.** *3.2.1. Influence on the Mechanical Properties of P1 and P3.* To quantitatively evaluate the influence of graphene substrate on the mechanical properties of P1, tensile tests were carried out on one representative peptide strand in P1 using the equilibrated configuration as the initial structure, and three independent tests were carried out on each case, respectively. Figure 9, panel a shows the comparison of the force versus the end-to-end distance curves for P1 with and without the graphene substrate. Under the mechanical loading, the peptide in helical structure twisted, and the hydrogen bonds along the $\alpha$-helix ruptured, which caused a sudden unfolding of helical turns. The rupture force is defined as the force when a sudden structural change occurs. It is seen from Table 2 that when the peptide is adsorbed onto the graphene substrate, the average rupture force increases from 2185.11 pN to 4646.17 pN. Hence, from both our structural analysis and mechanical test simulations, P1 shows improved mechanical properties with the graphene substrate, possessing higher rupture force and resilience. For example, without the graphene substrate, the resilience is found to be 18.88 kJ/ (mol nm$^3$). This value is found to increase to 58.07 kJ/ (mol nm$^3$) with the graphene substrate. Here, we define the resilience of the system as the energy stored before the rupture of hydrogen bonds. The influence on P3 is found to behave in a similar way, where both the rupture force and resilience increase when P3 is adsorbed to the graphene substrate (Figure 9c and Table 2). However, compared to P1, the increases in both the rupture force and the resilience of P3 are less significant (e.g., for P1, the rupture force is increased by 112.63% and the resilience by 207.57%; while for P3, the rupture force is increased by 46.82% and the resilience by 17.30%).

*3.2.2. Influence on the Mechanical Properties of P2.* The crystalline domain exhibits very stiff and brittle mechanical properties, and the pull-out test is an efficient way to evaluate the strength of the crystalline domain.[13] On the basis of the equilibrated structure, the strength of P2 is also evaluated by pulling out the central strand from the bottom layer away from the crystallite; the pull-out force versus the displacement curves for P2 is shown in Figure 9, panel b. The rupture force for pulling out the $\beta$-chain without graphene is 2114.67 pN, while with graphene, it is 2431.9 pN. These results are illustrated in Figure 9, panel b and Table 2. Although the graphene substrate perturbs the structural stability of the crystallite, its interaction

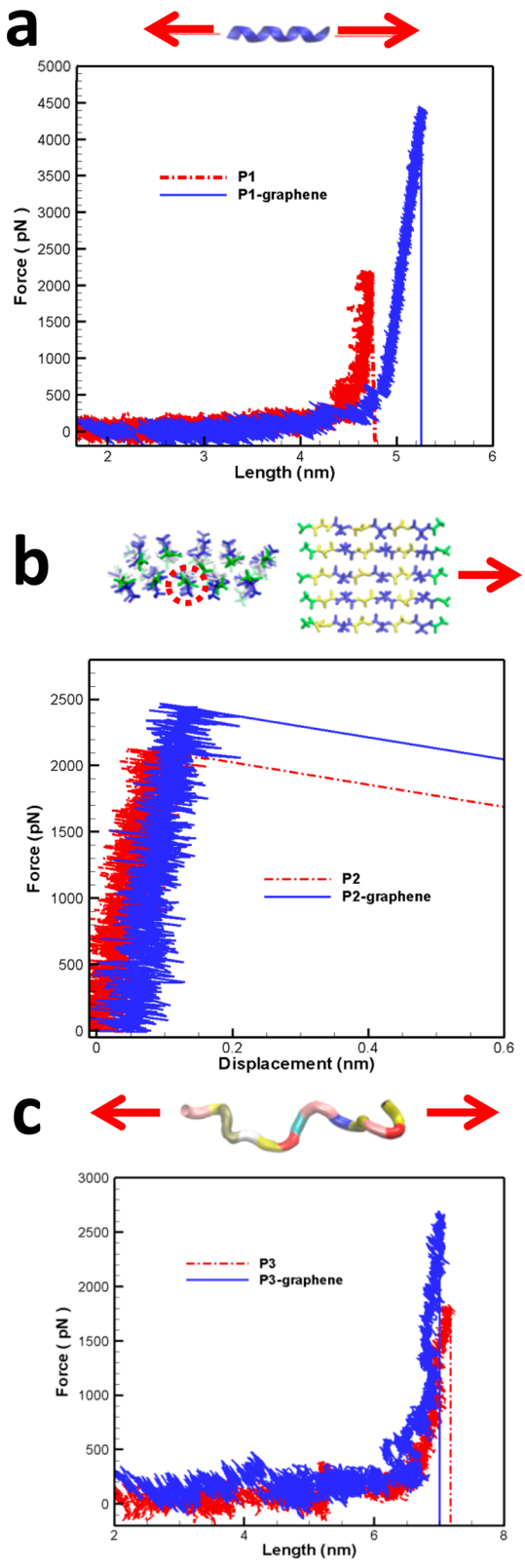


**Figure 9.** (a) Pulling force versus the end-to-end distance during tensile test of one of peptide strands in P1. (b) Pull-out force as the function of the displacement of P2. Side view and top view of the crystalline unit, with the $\beta$-chain to be pulled-out highlighted with an arrow. (c) Pulling force versus the end-to-end distance during tensile test of P3.



DOI: 10.1021/acsami.5b05615
ACS Appl. Mater. Interfaces 2015, 7, 21787–21796

Table 2. Rupture Force and the Resilience Calculated from the Tensile Tests on P1 and P3, and Pull-out Test for P2

| | structure | | | | | |
|---|---|---|---|---|---|---|
| mechanical properties | P1 | P1-graphene | P2 | P2-graphene | P3 | P3-graphene |
| rupture force (pN) | 2185.112 | 4646.17 | 2114.67 | 2431.90 | 1837.00 | 2697.05 |
| resilience (kJ/mol nm$^3$) | 18.88 | 58.07 | 14.12 | 19.60 | 83.32 | 97.74 |

with the graphene substrate enhances the strength of P2. Apparently, this enhancement in strength arises from the VDW interactions between the crystallite and the graphene substrate.

*3.2.3. Discussion.* The magnitude of the pulling rate used in this study (0.2 nm/ns) is relevant in many applications of the silk. In bioapplications, the speeds as high as ∼1 nm/ns are common to human body for running, throwing, jumping, etc.[55] The pulling rate and the spring constant adopted in the current study are reasonable and have been validated by earlier work.[45] Comparable values for these two parameters have also been adopted by previous works on mechanical properties of crystalline structures by several groups.[12−14] In particular, Xu et al.[14] investigated the influence of the pulling rate and the spring constant on the results of mechanical tests. It was reported that although the rupture force is slightly influenced by both the pulling rate and the spring constant, the rupture mechanisms of the crystallite observed at one pulling rate/spring constant repeated consistently across different pulling rates/spring constants. It was also reported in an earlier work that the unfolding mechanism of integrin $\alpha_V\beta_3$ ectodomain remained unchanged by using the different pulling parameters (including pulling rate and the spring constant).[56]

It is known that amorphous domains of silk fibroin, which are mainly composed of helical and random coil structures, contribute to the toughness of silk fibroin, while the crystalline domains play the dominant role in determining the strength of silk fibroin.[57] In this study, graphene is found to enhance both the strength and resilience of the protein. The enhancement in the mechanical properties of protein through interacting with graphene substrate depends on the sequence and structure of the protein. The present work suggests that the influence of graphene on the structural and mechanical properties of flexible domains such as helical and coil structures is more significant than that on stiff domains, such as $\beta$-sheets.

In the earlier works, Ou et al. showed that the dimers of a peptide experienced unfolding during their adsorption to graphene surfaces due to strong interactions between graphene and the peptide.[30] Katoch et al. demonstrated the complicated changes in the conformation of a dodecamer peptide during noncovalent interactions with graphene by using a combination of experimental and computational approach.[26] Zhang et al. reported that the stability of biological materials such as proteins and DNA could be enhanced significantly through their immobilization, interaction, or catalysis using graphene.[27] In our study, we examine the structural behavior of peptides at equilibrium states upon adsorption on graphene and their resulting changes in mechanical properties. Our study complements the earlier studies by providing new insights into the enhancement in the mechanical properties of peptides induced by graphene. It is hoped that our present study will inspire more researchers to work in this field and provide more numerical and experimental results.

It should be noted that the graphene could deform upon interaction with the peptides, and the graphene deformation could also be important in affecting structural and mechanical properties of the peptides. Considering the fact that simulating the deformability of the graphene and its interaction with the whole silk molecule requires tremendous computational resource, in the present work, we have chosen to fix the graphene and focus on the structural and mechanical behavior of silk fibroin. Our preliminary MD simulation on equilibrium runs of P4−graphene interaction without fixing the graphene shows that the trends in the changes of the secondary structure contents remain the same, that is, there is a drop in the $\beta$-sheet content and a slight increase in the helix content, indicating that whether the graphene is fixed or not will not affect the major conclusion of the present work.

In the present study, we have investigated the binding energy of peptides from different domains of silk fibroin to graphene as well as the changes in hydrogen-bond number and secondary structures of the peptides upon the adsorption. These results provide valuable information for the understanding of silk−graphene interaction at an equilibrium state. By performing tensile and pull-out tests, we have studied the effects induced by the graphene surface on the strength and resilience of the peptides, which provides valuable information about the mechanical behavior at the interface between the peptides and graphene substrate.

Our study demonstrated that complicated processes are involved when graphene interacts with different domains of silk fibroin. The understanding gained here regarding the changes in the conformational and mechanical properties of different domains of silk fibroin upon adsorption to graphene is a significant step toward understanding and manipulating their hybrid structures so as to further enhance the mechanical properties of silk fibroin.

## 4. CONCLUSION

We have performed MD simulations to investigate the effect of graphene substrate on the structure and mechanical properties of silk peptides. For protein domains with stable structure and strong intramolecular interactions (e.g., $\beta$-sheets), the graphene substrate tends to compete with the intramolecular interactions and thus may weaken the interchain interaction strength. For random or less ordered secondary structures and weak intramolecular interaction, the graphene substrate tends to enhance the stability of the peptide structures and increases/maintains the contents of more ordered structures (e.g., helical or $\beta$-sheet structures). It is also shown that the graphene substrate has the effect of enhancing the strength and resilience of different domains of silk fibroin. Both the structure and mechanical properties of amorphous/less ordered domains are more sensitive to the influence of graphene substrate. Our study provides a valuable reference for the rational design of bioinspired materials with enhanced mechanical properties.

## ■ ASSOCIATED CONTENT

### Supporting Information

The Supporting Information is available free of charge on the ACS Publications website at DOI: 10.1021/acsami.5b05615.

Complete sequence of P4 (PDF)



DOI: 10.1021/acsami.5b05615
ACS Appl. Mater. Interfaces 2015, 7, 21787−21796

## AUTHOR INFORMATION


### Corresponding Authors

*E-mail: my-han@imre.a-star.edu.sg.
*E-mail: zhangyw@ihpc.a-star.edu.sg.


### Author Contributions

‖These authors contributed equally to this work. The manuscript was written through contributions of all authors. All authors have given approval to the final version of the manuscript.

### Notes

The authors declare no competing financial interest.

## ACKNOWLEDGMENTS

This work was supported by the A*STAR Computational Resource Centre through the use of its high performance computing facilities. B.J. and D.L. thank the support from the National Science Foundation of China (Grant Nos. 11025208, 11221202, 11372042, and 11202026).

## REFERENCES


(1) Altman, G. H.; Horan, R. L.; Lu, H. H.; Moreau, J.; Martin, I.; Richmond, J. C.; Kaplan, D. L. Silk Matrix for Tissue Engineered Anterior Cruciate Ligaments. *Biomaterials* **2002**, *23*, 4131−4141.

(2) Yang, Y.; Chen, X.; Ding, F.; Zhang, P.; Liu, J.; Gu, X. Biocompatibility Evaluation of Silk Fibroin with Peripheral Nerve Tissues and Cells in Vitro. *Biomaterials* **2007**, *28*, 1643−1652.

(3) Liu, H.; Ge, Z.; Wang, Y.; Toh, S. L.; Sutthikhum, V.; Goh, J. C. Modification of Sericin-free Silk Fibers for Ligament Tissue Engineering Application. *J. Biomed. Mater. Res., Part B* **2007**, *82B*, 129−138.

(4) Lawrence, B. D.; Marchant, J. K.; Pindrus, M. A.; Omenetto, F. G.; Kaplan, D. L. Silk Film Biomaterials for Cornea Tissue Engineering. *Biomaterials* **2009**, *30*, 1299−1308.

(5) Gil, E. S.; Park, S. H.; Marchant, J.; Omenetto, F.; Kaplan, D. L. Response of Human Corneal Fibroblasts on Silk Film Surface Patterns. *Macromol. Biosci.* **2010**, *10*, 664−673.

(6) Gil, E. S.; Mandal, B. B.; Park, S. H.; Marchant, J. K.; Omenetto, F. G.; Kaplan, D. L. Helicoidal Multi-lamellar Features of RGD-functionalized Silk Biomaterials for Corneal Tissue Engineering. *Biomaterials* **2010**, *31*, 8953−8963.

(7) Tao, H.; Brenckle, M. A.; Yang, M. M.; Zhang, J. D.; Liu, M. K.; Siebert, S. M.; Averitt, R. D.; Mannoor, M. S.; McAlpine, M. C.; Rogers, J. A.; Kaplan, D. L.; Omenetto, F. G. Silk-based Conformal, Adhesive, Edible Food Sensors. *Adv. Mater.* **2012**, *24*, 1067−1072.

(8) Koh, L. D.; Cheng, Y.; Teng, C. P.; Khin, Y. W.; Loh, X. J.; Tee, S. Y.; Low, M.; Ye, E.; Yu, H. D.; Zhang, Y. W.; Han, M. Y. Structures, Mechanical Properties and Applications of Silk Fibroin Materials. *Prog. Polym. Sci.* **2015**, *46*, 86−110.

(9) Gatesy, J.; Hayashi, C.; Lewis, R. Extreme Diversity, Conservation, and Convergence of Spider Silk Fibroin Sequences. *Science* **2001**, *291*, 2603−2605.

(10) Takahashi, Y.; Gehoh, M.; Yuzuriha, K. Structure Refinement and Diffuse Streak Scattering of Silk (Bombyx mori). *Int. J. Biol. Macromol.* **1999**, *24*, 127−138.

(11) Nova, A.; Keten, S.; Pugno, N. M.; Redaelli, A.; Buehler, M. J. Molecular and Nanostructural Mechanisms of Deformation, Strength and Toughness of Spider Silk Fibrils. *Nano Lett.* **2010**, *10*, 2626−34.

(12) Keten, S.; Xu, Z.; Ihle, B.; Buehler, M. J. Nanoconfinement Controls Stiffness, Strength and Mechanical Toughness of Beta-sheet Crystals in Silk. *Nat. Mater.* **2010**, *9*, 359−367.

(13) Cheng, Y.; Koh, L. D.; Li, D.; Ji, B.; Han, M. Y.; Zhang, Y. W. On the Strength of $\beta$-sheet Crystallites of *Bombyx mori* Silk Fibroin. *J. R. Soc., Interface* **2014**, *11*, 20140305.

(14) Xu, C.; Li, D.; Cheng, Y.; Liu, M. S.; Zhang, Y. W.; Ji, B. Pulling out a Peptide Chain from $\beta$-sheet Crystallite: Propagation of Instability of H-bonds under Shear Force. *Acta Mech. Sin.* **2015**, *31*, 416−424.

(15) Shao, Z.; Vollrath, F. Surprising Strength of Silkworm Silk. *Nature* **2002**, *418*, 741.

(16) Liu, X. Y.; Du, N. *Enhanced Silk Protein Material Having Improved Mechanical Performance and Method of Forming the Same*. U.S. Patent 0,068,517 A1, September 12, 2007.

(17) Wu, X.; Liu, X. Y.; Du, N.; Xu, G.; Li, B. Unraveled Mechanism in Silk Engineering: Fast Reeling Induced Silk Toughening. *Appl. Phys. Lett.* **2009**, *95*, 093703.

(18) Wen, H.; Lan, X.; Zhang, Y.; Zhao, T.; Wang, Y.; Kajiura, Z.; Nakagaki, M. Transgenic Silkworms (Bombyx mori) Produce Recombinant Spider Dragline Silk in Cocoons. *Mol. Biol. Rep.* **2010**, *37*, 1815−1821.

(19) Castro Neto, A. H.; Guinea, F.; Peres, N. M. R.; Novoselov, K. S.; Geim, A. K. The Electronic Properties of Graphene. *Rev. Mod. Phys.* **2009**, *81*, 109−162.

(20) Novoselov, K. S.; Geim, A. K.; Morozov, S. V.; Jiang, D.; Katsnelson, M. I.; Grigorieva, I. V.; Dubonos, S. V.; Firsov, A. A. Two-Dimensional Gas of Massless Dirac Fermions in Graphene. *Nature* **2005**, *438*, 197−200.

(21) Terrones, M.; Botello-Mendez, A. R.; Campos-Delgado, J.; Lopez-Urias, F.; Vega-Cantu, Y. I.; Rodriguez-Macias, F. J.; Elias, A. L.; Munoz-Sandoval, E.; Cano-Marquez, A. G.; Charlier, J. C. Graphene for Electrochemical Sensing and Biosensing. *Nano Today* **2010**, *5*, 351−372.

(22) Wei, N.; Peng, X.; Xu, Z. Understanding Water Permeation in Graphene Oxide Membranes. *ACS Appl. Mater. Interfaces* **2014**, *6*, 5877−5883.

(23) Zhou, M.; Zhai, Y.; Dong, S. Electrochemical Sensing and Biosensing Platform Based on Chemically Reduced Graphene Oxide. *Anal. Chem.* **2009**, *81*, 5603−5613.

(24) Zhang, Y. Y.; Wang, C. M.; Cheng, Y.; Xiang, Y. Mechanical Properties of Bilayer Graphene Sheets Coupled by sp3 Bonding. *Carbon* **2011**, *49*, 4511−4517.

(25) Hu, K.; Gupta, M. K.; Kulkarni, D. D.; Tsukruk, V. V. Ultra-Robust Graphene Oxide-Silk Fibroin Nanocomposite Membranes. *Adv. Mater.* **2013**, *25*, 2301−2307.

(26) Katoch, J.; Kim, S. N.; Kuang, Z.; Farmer, B. L.; Naik, R. R.; Tatulian, S. A.; Ishigami, M. Structure of a Peptide Adsorbed on Graphene and Graphite. *Nano Lett.* **2012**, *12*, 2342−2346.

(27) Zhang, Y.; Wu, C.; Guo, S.; Zhang, J. Interactions of Graphene and Graphene Oxide with Proteins and Peptides. *Nanotechnol. Rev.* **2013**, *2*, 27−45.

(28) Gao, H. Probing Mechanical Principles of Cell−nanomaterial Interactions. *J. Mech. Phys. Solids* **2014**, *62*, 312−339.

(29) Zhou, R.; Gao, H. Cytotoxicity of Graphene: Recent Advances and Future Perspective. *Wiley Interdiscip. Rev.: Nanomed. Nanobiotechnol.* **2014**, *6*, 452−474.

(30) Ou, L.; Luo, Y.; Wei, G. Atomic-Level Study of Adsorption, Conformational Change, and Dimerization of an $\alpha$-Helical Peptide at Graphene Surface. *J. Phys. Chem. B* **2011**, *115*, 9813−9822.

(31) Cheng, Y.; Li, D.; Ji, B.; Shi, X.; Gao, H. Structure-based Design of Carbon Nanotubes as HIV-1 Protease Inhibitors: Atomistic and Coarse-Grained Simulations. *J. Mol. Graphics Modell.* **2010**, *29*, 171−177.

(32) Cheng, Y.; Zhang, Z.; Teo, Z. Deformation of Graphene Induced By Adsorption of Peptides: A Molecular Dynamics Study. *Int. J. Appl. Mech.* **2013**, *5*, 1350007.

(33) Qin, Z.; Buehler, M. J. Molecular Mechanics of Mussel Adhesion Proteins. *J. Mech. Phys. Solids* **2014**, *62*, 19−30.

(34) Qin, Z.; Buehler, M. J. Molecular Dynamics Simulation of the $\alpha$-Helix to $\beta$-Sheet Transition in Coiled Protein Filaments: Evidence for a Critical Filament Length Scale. *Phys. Rev. Lett.* **2010**, *104*, 198304.

(35) Li, D.; Ji, B.; Hwang, K.; Huang, Y. Crucial Roles of the Subnanosecond Local Dynamics of the Flap Tips in the Global Conformational Changes of HIV-1 Protease. *J. Phys. Chem. B* **2010**, *114*, 3060−3069.

(36) Li, T.; Oloyede, A.; Gu, Y. Adhesive Characteristics of Low Dimensional Carbon Nanomaterial on Actin. *Appl. Phys. Lett.* **2014**, *104* (2), 023702.




DOI: 10.1021/acsami.5b05615
*ACS Appl. Mater. Interfaces* 2015, 7, 21787−21796

(37) Zhou, C. Z.; Confalonieri, F.; Jacquet, M.; Perasso, R.; Li, Z. G.; Janin, J. Silk Fibroin: Structural Implications of a Remarkable Amino Acid Sequence. *Proteins: Struct., Funct., Genet.* **2001**, *44*, 119−122.
(38) Fossey, S. A.; Némethy, G.; Gibson, K. D.; Scheraga, H. A. Conformational Energy Studies of Beta-Sheets of Model Silk Fibroin Peptides. I. Sheets of Poly(Ala-Gly) Chains. *Biopolymers* **1991**, *31*, 1529−1541.
(39) He, Y. X.; Zhang, N. N.; Li, W. F.; Jia, N.; Chen, B. Y.; Zhou, K.; Zhang, J.; Chen, Y.; Zhou, C. Z. N-Terminal Domain of Bombyx mori Fibroin Mediates the Assembly of Silk in Response to pH Decrease. *J. Mol. Biol.* **2012**, *418*, 197−207.
(40) Wang, J.; Cieplak, P.; Kollman, P. A. How Well Does a Restrained Electrostatic Potential (RESP) Model Perform in Calculating Conformational Energies of Organic and Biological Molecules. *J. Comput. Chem.* **2000**, *21*, 1049−1074.
(41) Cornell, W. D.; Cieplak, P. B.; Bayly, C. I.; Gould, I. R.; Merz, K. M.; Ferguson, D. M.; Spellmeyer, D. C.; Fox, T.; Caldwell, J. W.; Kollman, P. A. A Second Generation Force Field for the Simulation of Proteins, Nucleic Acids, and Organic Molecules. *J. Am. Chem. Soc.* **1995**, *117*, 5179−5197.
(42) Hummer, G.; Rasaiah, J. C.; Noworyta, J. P. Water Conduction through the Hydrophobic Channel of a Carbon Nanotube. *Nature* **2001**, *414*, 188−190.
(43) Zou, J.; Ji, B.; Feng, X.; Gao, H. Self-Assembly of Single-Walled Carbon Nanotubes into Multi-Walled Carbon Nanotubes in Water: Molecular Dynamics Simulations. *Nano Lett.* **2006**, *6*, 430−434.
(44) Shi, X.; Cheng, Y.; Pugno, N. M.; Gao, H. Tunable Water Channels with Carbon Nanoscrolls. *Small* **2010**, *6*, 739−744.
(45) Xiao, S.; Stacklies, W.; Cetinkaya, M.; Markert, B.; Gräter, F. Mechanical Response of Silk Crystalline Units from Force-Distribution Analysis. *Biophys. J.* **2009**, *96* (10), 3997−4005.
(46) Hess, B.; Kutzner, C.; van der Spoel, D.; Lindahl, E. GROMACS 4: Algorithms for Highly Efficient, Load-Balanced, and Scalable Molecular Simulation. *J. Chem. Theory Comput.* **2008**, *4*, 435−447.
(47) Darden, T.; York, D.; Pedersen, L. Particle Mesh Ewald-An N.Log (N) Method For Ewald Sums In Large Systems. *J. Chem. Phys.* **1993**, *98*, 10089−10092.
(48) Humphrey, W.; Dalke, A.; Schulten, K. VMD: Visual Molecular Dynamics. *J. Mol. Graphics* **1996**, *14*, 33−38.
(49) Frishman, D.; Argos, P. Knowledge-based Protein Secondary Structure Assignment. *Proteins: Struct., Funct., Genet.* **1995**, *23*, 566−579.
(50) Jorgensen, W. L.; Chandrasekhar, J.; Madura, J. D.; Impey, R. W.; Klein, M. L. Comparison of Simple Potential Functions for Simulating Liquid Water. *J. Chem. Phys.* **1983**, *79*, 926−935.
(51) Sotomayor, M.; Schulten, K. Single Molecule Experiments in Vitro and in Silico. *Science* **2007**, *316*, 1144−1148.
(52) Guan, G.; Zhang, S.; Liu, S.; Cai, Y.; Low, M.; Teng, C. P.; Phang, I. Y.; Cheng, Y.; Duei, K. L.; Srinivasan, B. M.; Zheng, Y.; Zhang, Y. W.; Han, M. Y. Protein Induces Layer-by-Layer Exfoliation of Transition Metal Dichalcogenides. *J. Am. Chem. Soc.* **2015**, *137* (19), 6152−6155.
(53) Timar-Balazsy, A.; Eastop, D. *Chemical Principles of Textile Conservation*; Butterworth-Heinemann: Oxford, UK, 2002.
(54) Hardy, J. G.; Römer, L. M.; Scheibel, T. R. Polymeric Materials Based on Silk Proteins. *Polymer* **2008**, *49*, 4309−4327.
(55) in't Veld, P. J.; Stevens, M. J. Simulation of the Mechanical Strength of a Single Collagen Molecule. *Biophys. J.* **2008**, *95*, 33−39.
(56) Chen, W.; Lou, J.; Hsin, J.; Schulten, K.; Harvey, S. C.; Zhu, C. Molecular Dynamics Simulations of Forced Unbending of Integrin $\alpha V\beta 3$. *PLoS Comput. Biol.* **2011**, *7* (2), e1001086.
(57) Krasnov, I.; Diddens, I.; Hauptmann, N.; Helms, G.; Ogurreck, M.; Seydel, T.; Funari, S. S.; Müller, M. Mechanical Properties of Silk: Interplay of Deformation on Macroscopic and Molecular Length Scales. *Phys. Rev. Lett.* **2008**, *100* (4), 048104.


DOI: 10.1021/acsami.5b05615
*ACS Appl. Mater. Interfaces* 2015, 7, 21787−21796